Molecular dynamics of carrageenan composites reinforced with Cloisite Na^+ montmorillonite nanoclay

M.J. Sanchis[a], M. Carsí[a,b], M. Culebras[c], C.M Gómez[c], S. Rodriguez[d], F.G. Torres[d]

[a]*Department of Applied Thermodynamics, Institute of Electric Technology, Universitat Politècnica de València, Valencia, Spain*
[b]*Department of Applied Thermodynamics, Instituto de Automática e Informática Industrial, Universitat Politècnica de Valencia, 46022 Valencia, Spain*
[c]*Departament de Química Física, Institut de Ciència dels Materials, Universitat de València, Valencia, Spain*
[d]*Department of Mechanical Engineering, Pontificia Universidad Católica del Peru (Lima 32 - Peru)*

[*]Corresponding author: M.J. Sanchis; email: jsanchis@ter.upv.es

Keywords: carrageenan; dielectric relaxation spectroscopy, electric modulus, fragility

Nanocomposites comprising biodegradable carrageenan and glycerol (KCg) as the host polymer, with different contents of natural montmorillonite (MMT) as filler, were prepared by a solution casting process. Different techniques have been used to determine the interaction/behaviour among the different components of the samples such as Fourier transform infrared spectroscopy (FTIR), X-ray diffraction (XRD), Transmission electron microscope (TEM) and, mainly, Dielectric relaxation spectroscopy (DRS). FTIR indicates hydrogen interaction between carrageenan matrix and silicate that is confirmed by the XRD data indicating some kind of carrageenan intercalation between the MMT layers. A rather homogenous distribution of MMT into KCg matrix were observed using transmission electron microscopy. The MMT effect on the molecular mobility at the glass transition was studied by dielectric relaxation spectroscopy. The MMT addition resulted in a slower relaxation and a wider distribution of the relaxation times. The fragility index, *m*, increased upon MMT incorporation, which may be attributed to a reduction in mobility chains, due to the MMT confinement of the KCg network. In addition, the apparent activation energy associated with the relaxation dynamics of the chains at T_g increased with the MMT content. The modified films developed in this paper could be used to prepare biodegradable and edible packaging films and films for biomedical applications with improved mechanical and good dielectric response.

1. Introduction

Nanocomposites based on biopolymers and clays are environmental-friendly materials used for food packaging, biomedical and electromechanical applications (Hamzah et al., 2013; Rhim et al., 2013a; Rhim et al., 2014; Aranda et al., 2006). The addition of clay lead to a significantly enhanced thermal stability, mechanical properties and barrier properties of such nanocomposites (Shojaee-Aliabadi et al., 2014; Mahdavinia et al., 2012; Karadağ et al., 2014; Bitinis et al., 2011). Montmorillonite (MMT) is one of the most common alumino-silicates clays used as nanofiller. There are unmodified (Cloisite®Na^+) and organo-modified montmorillonites (Cloisite®30B, Cloisite®25A, Cloisite®20A) (Ramadan et al., 2010). Unmodified montmorillonite-Na (Cloisite®Na^+) has been used to prepare nanocomposites with a variety of biopolymers such a carrageenan (Rodriguez et al., 2016; Rhim et al., 2013b), agar (Rhim et al., 2011a, 2011b), chitosan (Darder et al., 2003), starch (Cyras et al., 2008; Almasi et al., 2010), among others.

Carrageenan is a naturally linear-sulfated polysaccharide extracted from red seaweeds. There are different types of carrageenan that differ in the position and number of the ester sulfate groups (Kirk et al. 1992). The most common type of carrageenan is kappa (κ), (iota) i- and lambda (λ)-carrageenan. Fred van de Velde (2008) reported the structural and functional properties of the κ/ι-hybrid carrageenan from different species of seaweeds. They found that the κ-fraction present in specimen *Chondracanthus Chamissoi* was 82%.

Carrageenan is one of the most abundant polysaccharides, which has strong gel forming ability, biocompatibility, and is environmentally friendly (Shankar et al. 2015). It is commonly used as thickening and stabilizing agent in prepared foods, cosmetics and pharmaceuticals. Carrageenan has also been used to prepare biodegradable and edible packaging films and films for biomedical applications (Shankar et al., 2015; Corvaglia et al., 2016a). However, low water vapor barrier and low mechanical properties are the main limitations of these carrageenan-based films.

In order to overcome these limitations, carrageenan-based nanocomposites using organic and non-organic reinforcements have been prepared. The reinforcements used improved the mechanical properties of the carrageenan-based films. For instance, Rodriguez et al., (2016) showed that the tensile strength of neat carrageenan films increased from 2.138 ± 0.720 MPa to 11.292 ± 1.212 MPa when reinforced with montmorillonite (5 wt%). Similarly, the elastic modulus of neat carrageenan films increased from 4.037 ± 0.760 MPa to 50.385 ± 5.671 MPa.

Shojaee-Aliabadi et al., (2014) prepared carrageenan-based films reinforced with Cloisite®Na^+, which exhibited improvement in physical, mechanical and water-vapor permeability properties when compared with pure carrageenan films. Jang et al. (2010) have reported the improvement of the mechanical and water vapor permeability of the red algae-nanoclay (Cloisite Na+) composites. XRD tests performed by Rhim et al., (2012) showed that the agar/κ-carrageenan- Cloisite® nanocomposites they prepared presented an intercalated structure. Similar results obtained for multilayer films

composed of polylactic acid and agar/κ-carrageenan-Cloisite® (Rhim et al., 2013b, Paul & Robenson, 2008) suggested that Cloisite® Na^+ is compatible with biopolymers due to the formation of interactions between polar hydroxyl groups and Na^+ ions of montmorillonite.

Dielectric relaxation spectroscopy (DRS) analysis was used to study the molecular dynamics in polymer nanocomposites based on carrageenan, cellulose, starch and other biopolymers (Sanchis et al., 2017; Boucher et al., 2012; Ortiz-Serna et al. 2011; Hernández et al., 2010). Different studies have reported that the effect of the clays on the molecular mobility of polymeric chains determine the dielectric properties of clay-based nanocomposites (Nikaj et al., 2010; Sengwa et al., 2010; Yi et al., 2007; Noda et al., 2005; Couderc et al., 2007; Wang et al., 2004). The DRS uniquely suited for the study of nanocomposite dynamics, due to that the ionic, interfacial, and dipole polarization produced when are placed in an electric field have significant different time and length scales (Kremer & Schönhals, 2003, Riande & Díaz-Calleja, 2004).

In this study, we have used carrageenan-based films, which can potentially be used as biodegradable packaging films and films for biomedical applications. The aim of this paper is to study the effect of montmorillonite (Cloisite®Na^+) on the molecular mobility of carrageenan composite films. FTIR, DRX, TEM and DRS spectroscopy were used to provide evidence for the presence of interaction between Cloisite®Na^+ and the carrageenan matrix.

2. Experimental

2.1. Materials

Chondracanthus Chamissoi was obtained from the Peruvian coast (Lima). Red algae were washed and stored at 2°C. Montmorillonite (Cloisite®Na^+) was purchased from ROCKWOOD ADITIVES (Louisville, USA). All chemicals were of analytical grade.

2.2. Extraction of polysaccharides

The extraction followed the method used by Tuvikene (Tuvikene et. al., 2006). Briefly, red algae were refluxed in a NaOH solution (1 M) for 4 hours at 90 °C using a magnetic stirrer. The suspension was then precipitated with 2-propanol, and the carrageenan was oven-dried at 40 °C. The carrageenan was washed three times with 2-propanol to remove salts and pigments.

2.3. Preparation of nanocomposite films

Films were prepared with various reinforcement contents (weight fraction (%): 5, 10 and 15) using a solution-intercalation method (Rhim et al., 2014; Mallakpour et al., 2012; Filippi et al., 2008). Cloisite®Na was precisely weighted, mixed into distilled water (100 mL), and stirred for 24 hours. The Cloisite®Na suspension was sonicated at 200 W for 10 min using ultra-probe sonicator (UP200Ht, Hielscher). Next, 1.0 g of carrageenan (KC) and 0.3 g of glycerol (g) were dissolved in 100 mL distilled water and added to the sonicated Cloisite®Na suspension. The carrageenan-Cloisite®Na suspension prepared above was mixed for approximately 1 hour at 90 °C using a

magnetic stirrer. The resulting solution (KCg) was poured evenly into plastic Petri dishes (100 x15 mm) and dried for approximately 24 hours at 40 °C. The chemical constitution of the nanocomposite samples, along with the MMT content, are depicted in Table 1.

Table 1 Sample code and weight fraction (%) MMT (Cloisite®Na^+) content, VFTH fit parameters, relative free volume, expansion coefficient, fragility index and activation energy associated with the glass-rubber relaxation at T_g of KCg/*x*MMT samples. The quantities with asterisk, m^* and $E_a{}^*(T_g)$, were calculated by empirical equations given in the text.

Sample code	**KCg**	**KCg/5MMT**	**KCg/10MMT**	**KCg/15MMT**
wt % MMT	**0**	**5**	**10**	**15**
τ_0 **(s)**	$10^{-12.1}\pm10^{0.1}$	$10^{-12.1}\pm10^{0.3}$	$10^{-12.0}\pm10^{0.4}$	$10^{-11.5}\pm10^{1.0}$
M(K)	2119.3±22.4	2070.8±18.6	2241.1±20.2	2350.3±63.3
T_v**(K)**	140.1±0.6	141.9±1.0	149.8±0.8	152.0±1.3
T_g^{DRS}**(K)(**τ**=100s)**	205.4	205.7	219.3	227.6
$\phi_g/B\times10^2$	2.83±0.02	2.90±0.01	2.68±0.01	2.55±0.02
$\alpha_g\times10^4$**,** K^{-1}	4.72±0.05	4.83±0.04	4.46±0.04	4.25±0.11
m	51.2±0.3	50.4±0.1	56.7±0.3	60.1±0.5
m*	65.0	48.7	50.9	51.6
$E_a(T_g)$**,** $kJ\cdot mol^{-1}$	196.0±1.3	194.9±0.5	227.7±1.0	243.9±2.2
$E_a{}^*(T_g)$**,** $kJ\cdot mol^{-1}$	205.3	209.6	229.0	234.7

2.4. Fourier transform infrared spectroscopy (FTIR)

Fourier transform infrared spectroscopy (FTIR) measurements were performed in a Nicolet Nexus FTIR spectrometer over the range 400–4000 cm^{-1} with the attenuated total reflectance accessory by co-addition of 60 scans with a spectral resolution of 2 cm^{-1}.

2.5. X-ray diffraction

X-ray diffraction analysis of samples were performed in a BRUKER-D8 FOCUS diffraction system, using Kα Cu (λ= 1.5406 Å) radiation and a PSD Lynxeye detector. The radiation was produced at 40 kV and 40 mA. Samples were analyzed over a 2θ range of 5-90° with a sampling interval of 0.04°. The d-spacing of the main peaks were calculated according to Bragg's law.

2.6. Morphological characterization (TEM)

Transmission electron microscope (TEM) samples were prepared by embedding a small piece of sample in Durcupan™ ACM resin (SigmaAldrich, Munich, Germany), curing overnight and then cutting cross sections using an Ultra 45 diamond knife (Diatome, Hatfield, PA). Samples were imaged on copper grids using a JEOL JEM-1010, coupled with a digital camera MegaView III at 100 kV.

2.7. Dielectric relaxation spectroscopy (DRS) characterization

The molecular dynamics of the KCg/*x*MMT (*x* = 5, 10 and 15) nanocomposites and native polymer (KCg) were determined by means of a Novocontrol Broadband Dielectric Spectrometer (Hundsagen, Germany) consisting of an Alpha analyzer to carry out measurements from 5×10^{-2} to 3×10^{6} Hz. This allows measurement of the complex dielectric permittivity, $\varepsilon^*(\omega)=\varepsilon'(\omega)-i\varepsilon''(\omega)$, where $\varepsilon'(\omega)$ and $\varepsilon''(\omega)$ are the storage and loss part of the dielectric permittivity. The temperature was controlled by a Novocontrol Quatro cryosystem with a precision of ±0.1 K during each sweep in frequency. The isothermal measurements were performed from -110 °C to 40 °C (step of 5 ºC) in an inert N_2 atmosphere to avoid moisture uptake. This temperature range was chosen because it covers the glass transition temperature and avoids other transitions that can experience the matrix with increasing temperature. Molded disc shaped samples of about 0.12 mm in thickness, with diameter of 10 mm, were mounted in the dielectric cell between two parallel gold-plated electrodes. The thickness of each sample was measured with a micrometer screw. In order to avoid an increase of conductivity due to water, the samples were initially dried at 40 °C in a vacuum oven until constant weight was reached. The experimental uncertainty was less than 5% in all cases.

In order to monitor the effect of the MMT content on the molecular dynamic of the KCg/*x*MMT (*x* = 5, 10 and 15) nanocomposites, we have carried out the analysis of dielectric spectra using the Havriliak-Negami (HN) empirical model (Havriliak & Negami, 1966 and 1967) in terms of dielectric modulus formalism, $M^*=1/\varepsilon^*$ (Moynihan, 1996; Tsangaris et al. 1998; Kremer & Schönhals, 2003). This analysis, that were carried out only for those peaks in the dielectric spectra for which the peak maximum was clearly discernible, results in data pairs (T, f_{max}) which are used to establish the relaxation map. In this sense, the analysis of the MMT content effect on the molecular mobility was carried out through the segmental relaxation time ($\tau=1/2\pi f_{max}$). This parameter provides information about the underlying microscopic phenomena, which are directly correlated with the macroscopic properties of the material.

As usual, the temperature dependence of the relaxation times for the α-relaxation is parameterized by means of the Vogel-Fulcher-Tammann-Hesse (VFTH) equation (Vogel, 1921; Fulcher, 1925; Tammann & Hesse, 1926)

$$\tau = \tau_0 \exp\left[\frac{M}{T-T_v}\right] \qquad (1)$$

where τ_0 is a pre-factor of the order of picoseconds, M is a material parameter defining its relaxation activation energy (energetic barrier to molecular rearrangement) and T_V is the Vogel temperature, about 50-70 K below T_g, currently associated with the temperature at which the entropies of the glassy systems and the crystal are similar; i.e., the configurational entropy of the glass system is nil. By comparing Eq. (1) with the Doolittle expression (Doolittle, 1951 and 1952), the relative free volume at the glass

temperature, $\phi_g/B = (T_g - T_v)/M$, and the expansion coefficient of the free volume, $\alpha_f = 1/M$ at T_g , can be evaluated.

In the 1980s Angell introduced the dynamic fragility index, m (Angell, 1985). This parameter that characterizes the rapidity with which the properties of the system vary as the temperature of a supercooled liquid approaches its glass transition temperature (Plazek & Ngai, 1991), can be evaluated based on the VFTH parameters as

$$m = \frac{M}{2.303 T_g \left(1 - T_v/T_g\right)^2} \qquad (2)$$

Fragile liquids show a steeper increment in relaxation times approaching glass transition than do strong liquids. Fragility values typically range between m = 16, for strong systems, and m = 200 for the fragile ones (Merino, E. et al., 2011). This parameter is of particular interest for polymeric systems, since it has a main role in the polymer processing.

The apparent activation energy associated with the relaxation dynamics of the chains at T_g can be obtained from the dynamic fragility index as $E_a(T_g) = 2.303 R m T_g$ (Sanchis M.J.et al. 2008). Accordingly, the higher T_g, the higher the activation energy.

3. Results and discussion

3.1. Fourier transform infrared spectroscopy (FTIR)

Fig. 1 shows the FTIR spectra of the carrageenan MMT composites. All the samples exhibited the typical vibrational modes of carrageenan in the range from 400 cm^{-1} to 4000 cm^{-1}. The band between 3000-3700 cm^{-1} corresponds with the -OH stretching, the bands centered at 2900 cm^{-1} and 2970 cm^{-1} are attributed to the C-H stretching related to the CH_2 and CH_3 groups of the carrageenan. The band centered at 1640 cm^{-1} can be attributed to the bending vibration of OH groups from absorbed water (Martins, J.T. et al., 2013). The band at 1400 cm^{-1} corresponds to the C-H bending. The stretching associated with the O=S=O bounds is located at 1230 cm^{-1}, the bands centered at 1078-1025 cm^{-1} correspond with the stretching vibration of C-O groups (C-OH and C-O-C ring group). At 840 cm^{-1} appears the band related to the C-O-S stretching in the sulfate groups (galactose-4-sulfate) (Rhim, J-W &Wang L-F, 2014; Martins, J.T. et al., 2013). There is a slight shift in the position of the band related to the stretching vibration of C-OH groups when the clay content increases in the films, as shows the vertical line in Fig. 1. The position of C-OH stretching vibration changes from 1025 cm^{-1} to 1010 cm^{-1} at 15% of clay content, attributed to the hydrogen bond interactions between carrageenan and MMT due to the presence of –OH groups in both materials (Martins, J.T. et al., 2013). In addition, a flatter maximum at higher MMT content in the -OH stretching band is observed. This fact can be explained due to the contribution of –OH bonds from the MMT. Hydrogen bonds and/or electrostatic interactions may have occurred between MMT and carrageenan as suggested by Martins et al (Martins, J.T. et al., 2013). Intercalation between carrageenan matrix and silicate layers can occur as

indicated in previous works (Rhim, J-W &Wang L-F, 2014) and agar nanocomposites (Rhim, J-W, 2011b).

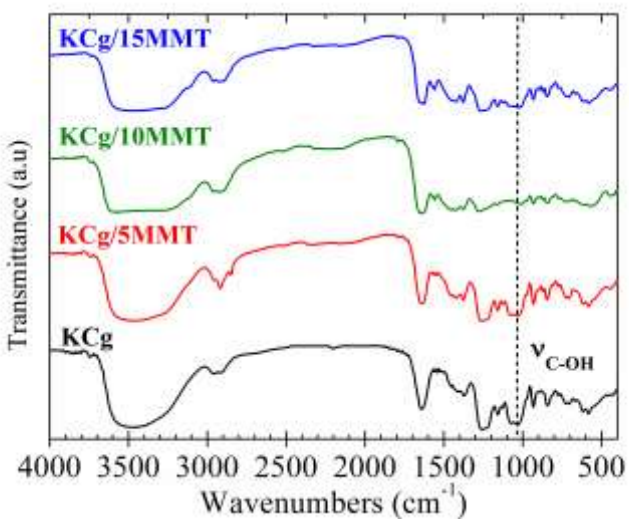

Fig. 1. FTIR spectra of KCg/*x*MMT nanocomposites.

3.2. X-Ray diffraction (XRD)

Fig. 2 shows the XRD spectra of the carrageenan MMT composites. The XRD spectrum of the pure carragenan (KCg) sample shows no diffraction peak due to the amorphous nature of carrageenan. The MMT sample shows a diffraction peak at 2θ=7.14°. A shift of this peak is observed for the KCg-MMT composite samples. Previous studies have reported that the intercalation of polysaccharides with clay increases the interlayer spacing of the clay, leading to a shift of the XRD peak towards the lower values of 2θ (Rhim et al., 2013; Rhim et al., 2014). Fig. 2 shows that the d-spacing of the MMT nanoclay increased from 1.24 nm to 1.73-1.80 nm in the carrageenan-based composites, suggesting that carrageenan chains entered into the silicate layers forming intercalated carrageenan/Cloisite®Na^+ nanocomposites. Similar behavior has been reported for carrageenan-based composite reinforced with Cloisite®30B (Martins et al., 2013) and Closite®Na+ (Rhim et al., 2013b).

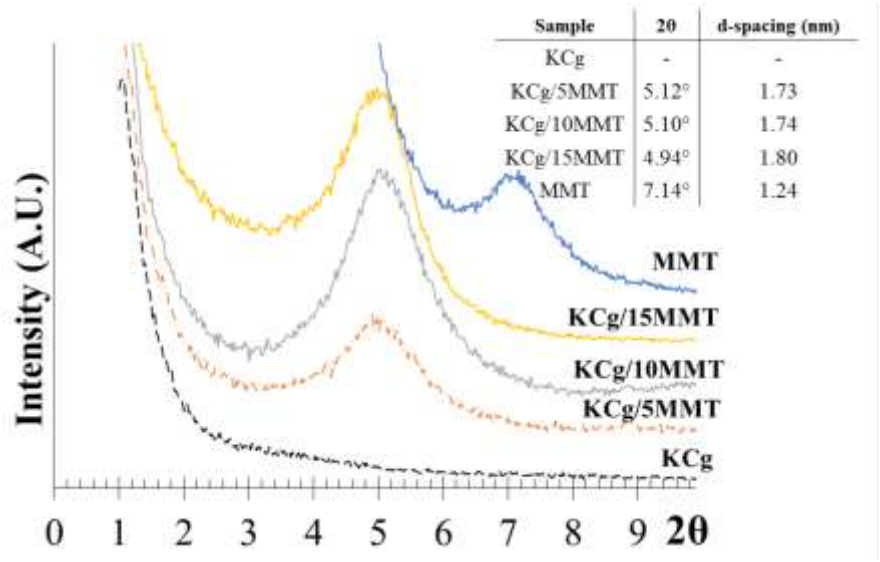

Fig. 2. XRD spectra of KCg/*x*MMT nanocomposites.

3.3. Morphological characterization

Fig. 3 shows representative transmission electron micrographs for KCg/15MMT nanocomposite. These images show a rather homogeneous distribution of the MMT into the KCg matrix, but only a poor dispersion, observing some agglomeration of the MMT in some zones.

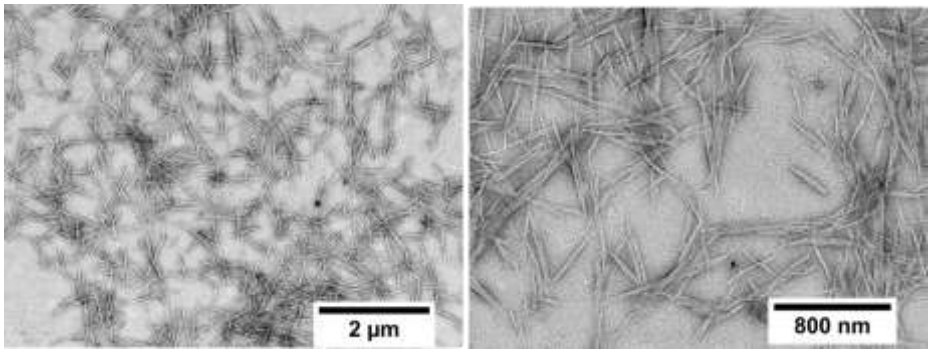

Fig. 3. TEM images of KCg/15MMT. A homogeneous distribution is observed.

3.4. Dielectric relaxation spectroscopy characterization

Isochrones showing the variation of the dielectric permittivity (ε') and dielectric loss (ε'') of KCg/*x*MMT nanocomposites with temperature, at several frequencies, are shown in Fig. 4. All the isochrones of the real component (ε') of the dielectric complex permittivity (ε^*) display the same pattern, a slight increase with temperature in the glassy state, followed by a steep increase at temperatures located in the vicinity of the glass transition temperature (glass rubber or α-relaxation) reaching a pseudoplateau. The isochrones at high temperatures depart from the plateau, undergoing a steep increase

with increasing temperature, as a consequence of the presence of electrode polarization (EP) phenomena, coming from the charge accumulation at the interface between sample and the electrode (Sauti et al. 2007). On the other hand, the dielectric loss isochrones exhibit at non well-defined absorption corresponding to the α-relaxation, followed by an increase at high temperature associated with the presence of conductive processes (ionic conductivity in conjunction with electrode polarization effects). Additionally, at low temperatures and high frequencies, further faster relaxation absorption (β-relaxation) was observed, for the samples with 10% and 15% wt MMT content. A slight decrease of the dielectric permittivity and low values for the dielectric loss were observed for the KCg/*x*MMT materials by increasing the amount of MMT nanoclay added. The decrease of the dielectric permittivity at low frequencies might be related to the exfoliated and intercalated clay ordered within the polymer matrix affecting the regular long chains of the polymer. The dipole orientation may be constrained making it difficult to move the chains due to the confinement of the nanoclay (Anastasiadis et al., 2000; Böhning et al., 2005).

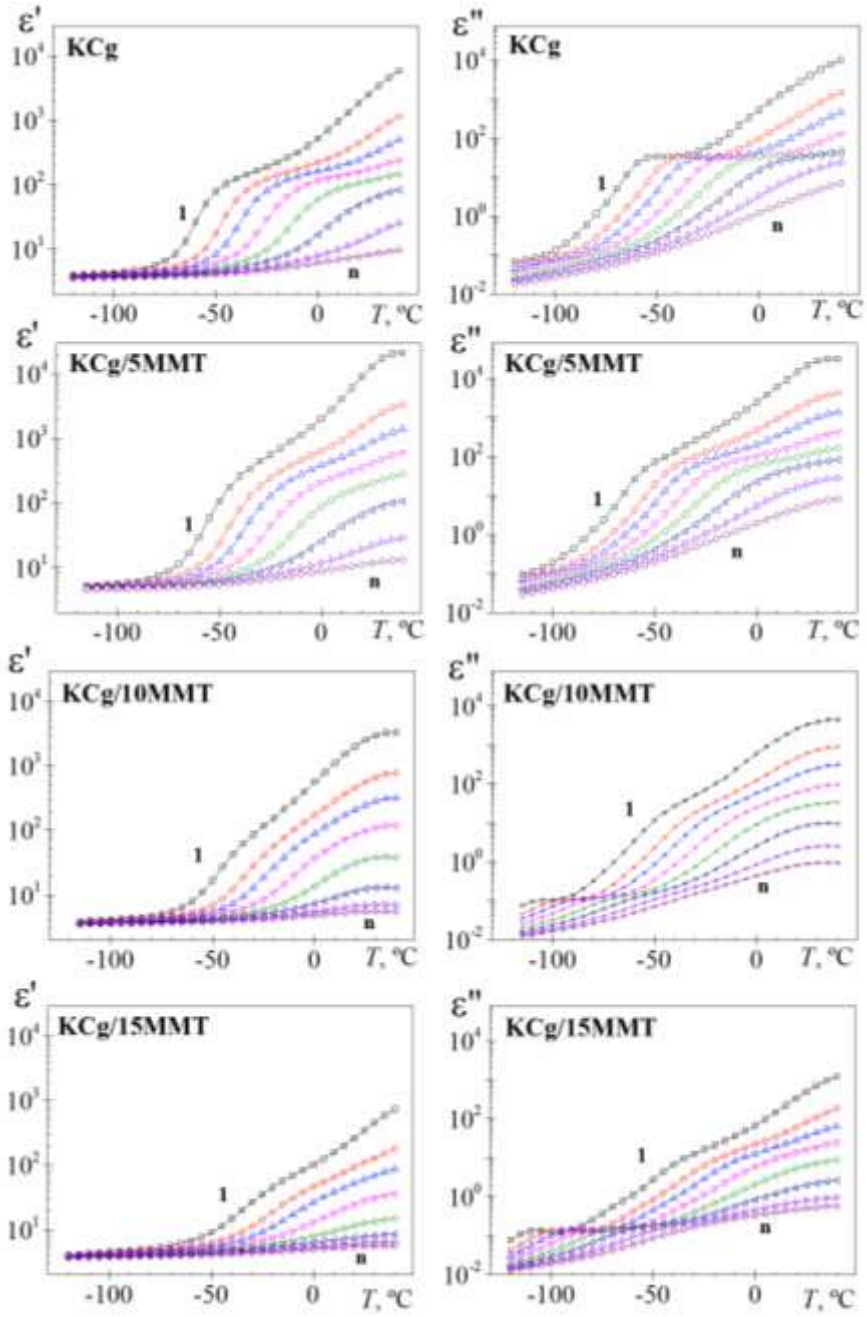

Fig. 4. Dielectric permittivity as a function of temperature for KCg/*x*MMT nanocomposites at several frequencies: 4.92×10^{-2}, 1.19×10^{0}, 8.72×10^{0}, 9.5×10^{1}, 1.04×10^{3}, 1.13×10^{4}, 1.24×10^{4} and 9.08×10^{5} Hz.

The frequency dependence of the dielectric permittivity (ε') and dielectric loss (ε''), at several temperatures, are presented in Fig. 5. As usual, ε' increases as frequency decreases reaching a pseudo-plateau corresponding to the relaxed dipoles. However, after the plateau and as the frequency decreases further, ε′ increases again due to the electrode polarization (EP) phenomena derived from the accumulation of charges at the electrode-polymer interface. At low frequency, ε′ values increase with the inclusion of 5%wt MMT, however for higher content a decrease of the permittivity is observed. The dielectric loss isotherms in the frequency domain, shown in Fig. 5, present two dipolar

relaxation processes: at high frequencies a secondary relaxation labelled as β and at low frequencies an absorption associated with the glass-liquid or α-relaxation. The last relaxation is progressively dominated by the conductive contribution as the temperature and frequency increase and decrease, respectively.

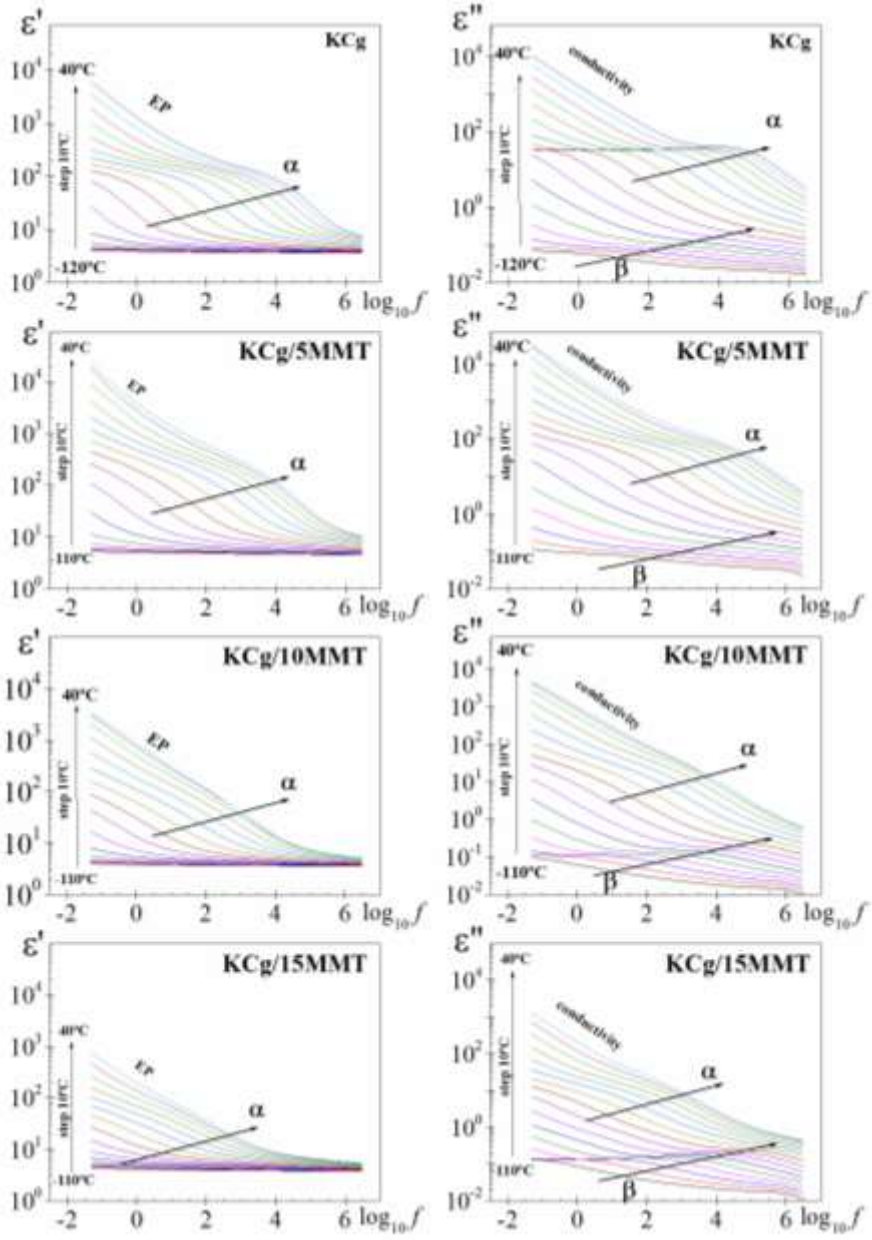

Fig. 5. Frequency dependence of the real and imaginary parts of the complex dielectric permittivity for KCg/*x*MMT nanocomposites at several temperatures.

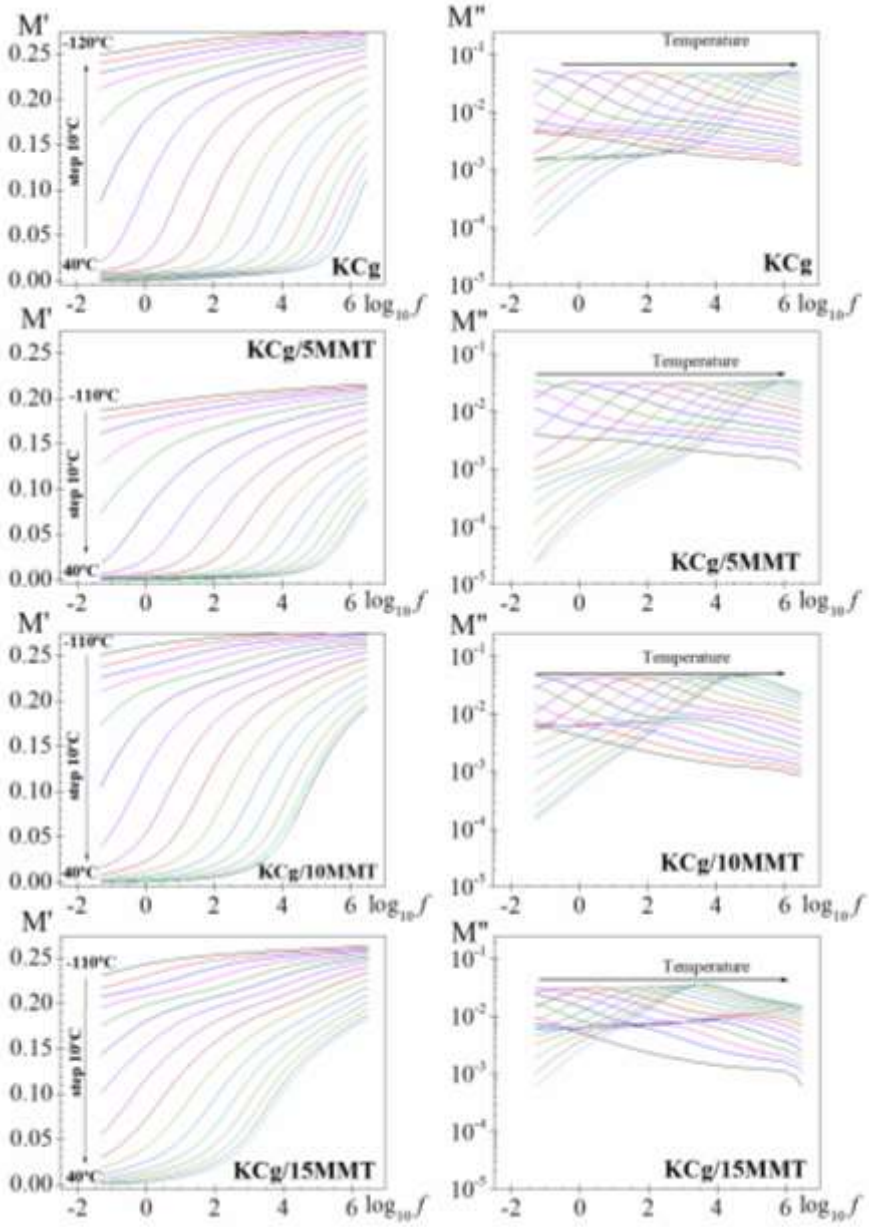

Fig. 6. Frequency dependence of the real and imaginary parts of the complex dielectric modulus for KCg/*x*MMT nanocomposites at several temperatures.

The reciprocal permittivity or electric modulus ($M^*=1/\varepsilon^*$) formalism can be used to a better description of the relaxation processes (Macedo et al. ,1972; Kremer & Schönhals, 2003). This representation presents several advantages, such as: (i) better resolution observed for dipolar and conductive processes since at low frequencies the imaginary part of the electric modulus shows a peak whereas the loss factor exhibits a sharp monotonic increase (Macedo et al.,1972) and (ii) negligible contribution of electrode polarization effects, allowing the evaluation of relaxation processes at the low frequency range of the dielectric spectra (Tsangaris et al., 1998; Psarras et al., 2007). The real (M') and the imaginary (M'') parts of the electric modulus (M^*) of samples as a function of frequency over a selected range of temperatures (-110 º to -40 ºC) are shown in Fig. 6. At lower frequencies, the M' is approaching toward zero at all temperatures,

suggesting the negligible electrode polarization (EP) contribution for the electric modulus. With increasing frequency, their value increases, reaching an asymptotic value at higher frequencies. This change is associated to the relaxation process. At high temperatures, two processes were observed in M'' spectra, corresponding, in increasing order of frequency, to the conductivity and glass-liquid or α-relaxation processes. At low temperatures, a non-well defined secondary process was observed. The peak maximum shifts toward higher frequencies with increasing temperature, suggesting that there is an increase in relaxation rate due to the thermal activation of the implicated processes.

In order to establish a better comparison of the effect of the inclusion of MMT, in Fig. 7 are represented the temperature and frequency dependence of the ε'' and M'' at 1 Hz and 0 ºC, respectively for the four samples analyzed. As we can observe in Fig. 7a, at 1 Hz two dipolar relaxations processes were observed in the temperature dependence of the ε'' spectra. By increasing the MMT content, the definition of the β-relaxation and α-relaxation improves and worsens, respectively. Both, dipolar and conductive processes are more clearly defined in the M'' representation. The same effect is depicted in Fig. 7b, where the steady increase in the isotherm ε'' representation, at low frequency, converted in a peak in M'' representation. This peak, associated with the conductivity process, is better defined for the sample without and with lower MMT content. The dipolar relaxation peaks (M'') appears shifted to higher frequencies with respect to permittivity representation (ε''), as would be expected, [$(\tau_\varepsilon/\tau_M) = (\varepsilon_0/\varepsilon_\infty)$, where ε_0 and ε_∞ denote the unrelaxed and relaxed parts of the ε', respectively].

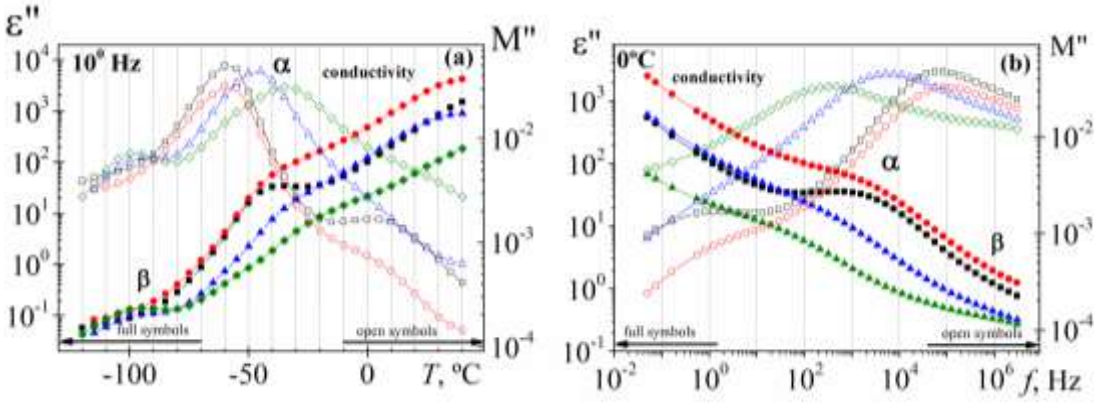

Fig. 7. Temperature (a) and frequency (b) dependence of ε'' and M'' at 1 Hz and 0ºC, respectively. [square (KCg), circle (KCg/5MMT), triangle (KCg/10MMT) and diamond (KCg/15MMT)].

The maxima peak of dipolar processes shifts to high temperature and low frequency by addition of MMT nanoclay. On the other hand, the peak height, which can be related to the interfaces properties (the stronger KCg/MMT interface, the lower the energy dissipation), decreases by increasing the MMT content. Thus, incorporation of MMT nanoclay restricts the movement of the polymer molecules near to the MMT surface. Another interesting result is the broadening of the loss curve when the MMT content

increases. This observation probably is associated with the difference in the physical state of the KCg matrix surrounding the MMT nanoclay to the rest. In other words, the KCg mobility near MMT nanoclay is different from the mobility of the neat KCg, which leads to wider relaxation spectra, and therefore to a relaxation broadening.

The HN parameters were determined at several temperatures from a multiple nonlinear regression analysis of the experimental data of the imaginary part of the electric modulus (M'') allowing the characterizing peak parameters to vary. This analysis were carried out for several isotherms of each one of the sample, KCg/*x*MMT (x = 0, 5, 10 and 15). In the temperature range analyzed, the shape parameters, a_{HN} and b_{HN}, lie in the range [0.52-0.89] and [0.39-0.75], respectively. The a_{HN} shape parameter, which relates to the broadness of the relaxation curve (the higher the a_{HN} parameter, the narrower the relaxation peak is), decreases by increasing the MMT content. Therefore, the distribution of relaxation times increases by increasing the MMT content. This behavior can be associated to the packed chain effect (Sartori Pompeo da Silva et al., 2014). The presence of MMT broadens the glass rubber relaxation because of the movement restrictions in the KCg chains segments near the MMT nanoclay. Thus, the movement of the chain segments of distinct zones is different in time/temperature scale, causing a broadening of the relaxation spectrum.

On the other hand, the b_{HN} shape parameter, which relates to the symmetry of the relaxation peak, increases by increasing the MMT content. Although, for amorphous polymers, a non-symmetric distribution of relaxation times is expected for the α relaxation ($b_{HN} < 1$), several systems such as semicrystalline polymers, composites, blends, copolymers and more generally for heterogeneous systems, a symmetrical distribution ($b_{HN}=1$) has been observed for the α relaxation processes (Ortiz-Serna et al, 2011; Redondo-Foj et al., 2014; Boyd, 1985; Laredo et al, 2003; Ryabov & Nuriel, 2003; Janik & Paluch, 2001; Feldman et al. 2002; Noda, 2005). In our case, the b_{HN} parameter not was equal to one, but its value increases by increasing the MMT content.

In order to analyze the MMT content effect in the molecular dynamic of the samples, the temperature dependence of the relaxation times has been plotted in Fig. 8. This dependence moves away from Arrhenius behavior, following a dependence of VFTH type. Values of the parameters that fit VFTH equation to the experimental results are collected in Table 1. Based on the empirical observation that T_v is usually about 50-70 °C below the glass transition temperature, the latter can also be pinpointed. However, the value of T_g is conventionally determined as the temperature at which the relaxation time of the segmental relaxation is 100s, an arbitrarily long time (Kremer & Schönhals, 2003). By using this last criterion, the obtained T_g values show an increase of the same with MMT content. Thus, the evaluated T_g of composites (205.7-227.6 K) was slightly higher than that of the neat carrageenan matrix (205.4 K). The slow dynamics observed, by increasing the MMT content, can be related to the restricted chain molecular mobility in the interfacial region, in which polymer chains are effectively interacted to the MMT surface. In this sense, the build-up of T_g can be considered as a measure of the interfacial interaction. Attractive NP-polymer interactions increase T_g, whereas a

reduction is expected when non-attractive polymer-NP interactions are presented (Lu & Nutt, 2003; Pazmiño Betancourt, et. al, 2013).

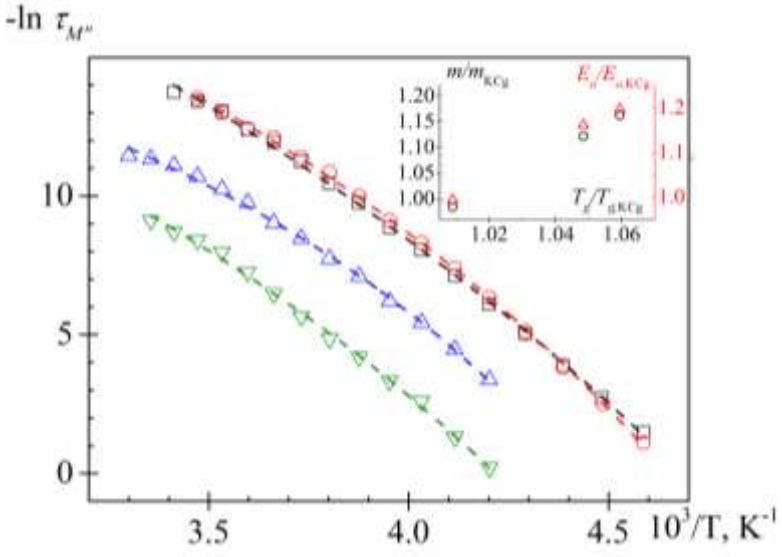

Fig. 8. Temperature dependence of the relaxation times for KCg/*x*MMT samples [KCg (square), KCg/5MMT (circle), KCg/10MMT (up triangle) and KCg/15MMT (down triangle)]. Lines represent the fitting. Inset: Parametric plots of (left) the relative fragility m/m_{KCg} vs $T_g/T_{g,KCg}$ and (right) the relative activation energy $E_a/E_{a,KCg}$ vs $T_g/T_{g,KCg}$

The relative free volume at the glass temperature, ϕ_g/B, and the expansion coefficient of the free volume, α_f, evaluated (collected in Table 1**)** are in agreement with those reported for other flexible polymers which lie in the vicinities of $2.5 \times 10^{-2} \pm 5.0 \times 10^{-3}$ and $(4-6) \times 10^{-4}$ K^{-1}, respectively (Ferry, 1980). When 5% wt MMT was incorporated in the KCg matrix, an increase of both parameters was observed. Moreover, a slight reduction in both parameters was observed by increasing the MMT content in the composite. This result can be related with the increase interaction between MMT and KCg matrix by increasing the MMT content.

To compare the temperature dependence of the relaxation times, the Angell's fragility concept (Angell, 1985) was applied to samples with different MMT content. Greater fragility is usually linked with a wider segmental dispersion. The calculated dynamic fragility index (*m*), based on the VFTH parameters, *vs*. MMT content are presented in Table 1. A moderate increase in the dynamic fragility index by raising the MMT content is observed. These results highlight out that a slight decrease in the chains mobility due to MMT dwelling of the carrageenan network, is produced. In addition, the increase in fragility compared to the neat KCg can also be promoted by the presence of interactions between components of the composites (Pazmiño Betancourt, et. al, 2013). Inset in Fig. 8 confirms that T_g and *m* vary proportionally, according to the empirical equation proposed for Qin and McKenna, $m^* = 0.28(\pm 0.067)T_g + 9(\pm 20)$ (Qin & McKenna, 2006). The values of *m** calculated by the former expression, shown in Table 1, are in rather good agreement with those obtained from Eq. (2).

A similar proportionality can be expected between T_g and E_a, since both should be proportional to the scale of interactions. The results for the activation energy associated with the glass-rubber relaxation at T_g, collected in Table 1, also increases by increasing the MMT content. The values obtained are in agreement with those predicted by the empirical model equation proposed for Qin and McKenna (Qin & McKenna, 2006), $E_a^*(T_g)$ = [0.006T_g^2 (K) - 35] kJ/mol), reported in the last line of Table 1.

4. Conclusions

Nanocomposites based on carrageenan (KC) are a growing research issue due to their good biodegradability. In this study, natural montmorillonite (MMT)**,** Cloisite® Na^+ was used as a nanoclay. The effect of the MMT content on the properties of KCg-MMT composites was investigated by means of TEM, FTIR, XRD and DRS techniques. The good distribution of the MMT in the KCg matrix was demonstrated by TEM. The intermolecular interactions between the KCg and MMT components, verified by FTIR, affected significantly the molecular mobility as have been verified by DRS.

DRS has been evidenced to be a formidable technique for investigating molecular dynamics of KCg/*x*MMT nanocomposites. By using the electric modulus formalism, we have analyzed the influence of MMT on the molecular mobility, at the glass transition, of the composites. The temperature/frequency of the maximum, the intensity and the broadness of the glass rubber transition, or α-relaxation process, are altered as the MMT content increases:

i. The α-relaxation process is shifted to higher temperatures and lower frequencies (up to two orders of magnitude compared to the unfilled polymer) by addition of MMT nanoclay. The evaluated T_g from DRS increases from 205.4 K (KCg) to 227.6 K with the incorporation of a 15% wt of MMT. These trends indicate a decrease of molecular mobility by increasing the MMT content.
ii. The height of the peak decreases by increasing the MMT content. Thus, incorporation of MMT nanoclay restricts the movement of the polymer molecules near the MMT surface. This fact is in good accordance with FTIR results and with the values obtained for the relative free volume and the fragility index, *m*, which indicate a reduction in mobility chains, due to the MMT confinement into the carrageenan network.
iii. The a_{HN} shape parameter, which is indicative of a widening of the relaxation curve (the higher value, the smaller broadness) decreases by increasing the MMT content. Therefore, the distribution of relaxation times, as well as the broadness of the α-relaxation process increases by increasing the MMT content. This result is related to the fact of the movement of the chain segments of distinct zones is different in time/temperature scale. Thus, the chain polymer mobility near MMT nanoclay is different from the mobility of the pure polymer. A decrease in the a_{HN} shape parameter is linked with the increase in the fragility index value. These results are associated with an increase of the heterogeneity of the relaxation environment and

of the interfacial adhesion between the composite components (nanoclay and matrix). The heterogeneity increase leading to a more fragile system.

Acknowledgements

This work was supported by the DGCYT [MAT2015-63955-R]; the Vice-Rectorate for Research of the Pontificia Universidad Católica del Perú and the National Council of Science, Technology and Technological Innovation of Peru (CONCYTEC/FONDECYT).

References

Almasi, H., Ghanbarzadeh, B., & Entezami, A. A. (2010). Physicochemical properties of starch–CMC–nanoclay biodegradable films. *International Journal of Biological Macromolecules*, 46(1), 1-5.

Anastasiadis, S. H., Karatasos, K., Vlachos, G., Manias, E., & Giannelis, E. P. (2000). Nanoscopic-Confinement Effects on Local Dynamics. *Physical Review Letter*, 84, 915.

Angell, C. A. (1985). Strong and fragile liquids, in Relaxations in Complex Systems, K. L. Ngai and G. B. Wright, Eds., pp. 3–11, NRL, Washington, DC, USA.

Aranda, P., Darder, M., Fernández-Saavedra, R., López-Blanco, M., & Ruiz-Hitzky, E. (2006). Relevance of polymer–and biopolymer–clay nanocomposites in electrochemical and electroanalytical applications. *Thin Solid Films*, 495(1), 104-112.

Bitinis, N., Hernández, M., Verdejo, R., Kenny, J. M., & Lopez-Manchado, M. A. (2011). Recent advances in clay/polymer nanocomposites. *Advanced Materials*, 23(44), 5229-5236.

Böhning, M., Goering, H., Fritz, A., Brzezinka, K-W., Turky, G., Schönhals, & A., Schartel, B. (2005). Dielectric Study of Molecular Mobility in Poly(propylene-graft-maleic anhydride)/Clay Nanocomposites. *Macromolecules*, 38, 2764-2774.

Boucher, V.M., Cangialosi, D., Alegría, A., & Colmenero, J. (2012). Time dependence of the segmental relaxation time of poly(vinyl acetate)-silica nanocomposites. *Physical Review E*, 86, 011501.

Boyd, R.H. (1985). Relaxation processes in crystalline polymers: experimental behavior. *Polymer,* 26(3), 323–347.

Cyras, V. P., Manfredi, L. B., Ton-That, M. T., & Vázquez, A. (2008). Physical and mechanical properties of thermoplastic starch/montmorillonite nanocomposite films. *Carbohydrate Polymers*, 73(1), 55-63.

501 Corvaglia, S., Rodríguez, S., Bardi, G., Torres, F. G., & López, D. (2016). Chitin
502 whiskers reinforced carrageenan films as low adhesion cell substrates. *International*
503 *Journal of Polymeric Materials and Polymeric Biomaterials*, 65(15), 574-580.

504 Couderc, H., Delbreilh, L., Saiter, A., Grenet, J., De Souza, N., & Saiter, J.M. (2007).
505 Relaxation in poly-(ethylene terephthalate glycol)/montmorillonite nanocomposites
506 studied by dielectric methods. *Journal of Non-Crystalline Solids* 353, 4334–4338.

507 Darder, M., Colilla, M., & Ruiz-Hitzky, E. (2003). Biopolymer-clay nanocomposites
508 based on chitosan intercalated in montmorillonite. *Chemistry of Materials*, 15(20),
509 3774-3780.

510 Doolittle, A. K. (1951). Studies in Newtonian Flow. II. The Dependence of the
511 Viscosity of Liquids on Free-Space. *Journal of Applied Physics* 22, 1471.

512 Doolittle, A. K. (1952). Studies in Newtonian Flow. III. The Dependence of the
513 Viscosity of Liquids on Molecular Weight and Free Space (in Homologous Series).
514 *Journal of Applied Physics* 23, 236.

515 Feldman, Y., Puzenko, A., & Ryabov, Y. (2002). Non-Debye dielectric relaxation in
516 complex materials. *Chem. Phys.* 284 (1-2),139–168.

517 Ferry, JD. Viscoelastic Properties of Polymers. New York: Wiley 1980:264

518 Filippi, S., Marazzato, C., Magagnini, P., Famulari, A., Arosio, P., & Meille, S. V.
519 (2008). Structure and morphology of HDPE-g-MA/organoclay nanocomposites:
520 Effects of the preparation procedures. *European Polymer Journal* 44, 987–1002.

521 Fulcher, G.S. (1925). Analysis of recent measurements of the viscosity of glasses.
522 *Journal of the American Ceramic Society*, 8 (6), 339-340.

523 Hamzah, H. M., Osman, A., Tan, C. P., & Ghazali, F. M. (2013). Carrageenan as an
524 alternative coating for papaya (Carica papaya L. cv. Eksotika). *Postharvest Biology*
525 *and Technology*, 75, 142-146.

526 Havriliak S. & Negami S. (1966). A complex plane analysis of α-dispersions in
527 some polymer systems. *J Polym Sci, Polym Symp*, *14*, 99-117.

528 Havriliak, S. & Havriliak S. (1967). *Dielectric and Mechanical Relaxation in*
529 *Materials*, Hanser: Munich.

530 Hernández, M., Carretero-González, J. , Verdejo, R., Ezquerra, T. A., López-
531 Manchado, M. A. (2010). Molecular Dynamics of Natural Rubber/Layered
532 Silicate Nanocomposites As Studied by Dielectric Relaxation Spectroscopy,
533 *Macromolecules*, 43, 643-651

534 Jang, S.-A., Lim G.-O., Song K. B. (2010). Use of nano-clay (Cloisite Na+)
535 improves tensile strength and vapour permeability in agar rich red algae
536 (Gelidium corneum)– gelatin composite films, *International Journal of Food and*
537 *Technology*, 45, 1883-1888.

538 Janik, P., Paluch, M., Ziolo, J., Sulkowski, W. Nikiel, L. (2001). Low-frequency
539 dielectric relaxation in rubber. *Physical Review E*, 64, 042502.

540 Karadağ, E., Hasgül, B., Kundakci, S., & Üzüm, Ö. B. (2014). A study of polymer/clay
541 hybrid composite sorbent-based AAm/SMA hydrogels and semi-IPNs composed of
542 ι-carrageenan and montmorillonite for water and dye sorption. *Advances in Polymer*
543 *Technology*, 33(4).

544 Kirk, R.E., Othmer, D.F. in: I Kroschwitz, M Howe-Grant (Eds.), *Encyclopedia of*
545 *Chemical Technology*, 4th ed., vol. 4, Wiley, New York, NY, 1992, pp. 942–961.

546 Kremer, F.; Schönhals, A. (2003). In Broadband Dielectric Spectroscopy; Springer:
547 Berlin.

548 Laredo, E., Grimau, M., Sánchez, F. Bello, A. (2003). Water Absorption Effect on the
549 Dynamic Properties of Nylon-6 by Dielectric Spectroscopy, *Macromolecules,* 36
550 (26), 9840–50.

551 Lu, H., Nutt, S. (2003). Restricted Relaxation in Polymer Nanocomposites near the
552 Glass Transition. *Macromolecules*, 36, 4010-4016.

553 Macedo, P.B., Moynihan, C.T., Bose, R. (1972). The role of ionic diffusion in
554 polarization in vitreous ionic conductors. *Phys Chem Glasses*, 13,171–179.

555 Mahdavinia, G. R., Massoudi, A., Baghban, A., & Massoumi, B. (2012). Novel
556 carrageenan-based hydrogel nanocomposites containing laponite RD and their
557 application to remove cationic dye. *Iranian Polymer Journal*, 21(9), 609-619.

558 Mallakpour, S., Dinari, M. (2012). Biomodification of Cloisite Na^+ with L-Methionine
559 Amino Acid and Preparation of Poly(vinyl alcohol)/Organoclay Nanocomposite
560 Films. *Journal of Applied Polymer Science*, 124, 4322–4330.

561 Martins, J. T., Bourbon, A. I., Pinheiro, A. C., Souza, B. W. S., & Cerqueira, M. A.,
562 Vicente A. A. (2013). Biocomposite Films Based on κ-Carrageenan/Locust Bean
563 Gum Blends and Clays: Physical and Antimicrobial Properties. *Food and Bioprocess*
564 *Technology* 6, 2081–2092

565 Merino, E. G., Atlas, S., Raihane, M., Belfkira, A., Lahcini, M., Hult, A., Dionísio, M.,
566 & Correia, N. T. (2011). Molecular dynamics of poly(ATRIF) homopolymer and
567 poly(AN-co-ATRIF) copolymer investigated by dielectric relaxation spectroscopy.
568 *European Polymer Journal*, 47(7), 1429− 1446.

569 Moynihan, C.T. (1996). Analysis of electrical relaxation in ionically conducting glasses
570 and melts. *Journal of Non-Crystalline Solids*, 203, 359-363.

571 Nikaj, E., Stevenson-Royaud, I., Seytre, L., & Espuche, E. (2010). Dielectric properties
572 of polyamide 6-montmorillonite nanocomposites. *Journal Non-Crystalline Solids,*
573 356, 589–596.

574 Noda, N., Lee, Y-H., Bur, A.J., Vivek, M., Snyder, C.R. Roth, S.C., & McBrearty, M.
575 (2005). Dielectric properties of nylon 6/clay nanocomposites from on-line process
576 monitoring and off-line measurements. *Polymer*, 46 (18), 7201-7217.

577 Ortiz-Serna, P.,Díaz-Calleja, R.,Sanchis, M.J., Riande, E., Nunes, R., Martins, A., &
578 Visconte, L. (2011). Dielectric spectroscopy of natural rubber-cellulose II
579 nanocomposites. *Journal Non-Crystalline Solids,* 357, 598–604.

580 Psarras, G. C., Gatos, K. G., & Karger-Kocsis, J. (2007). Dielectric Properties of
581 Layered Silicate-Reinforced Natural and Polyurethane Rubber Nanocomposites. *J.*
582 *Appl. Polym. Sci.,* 106 (2), 1405–1411.

583 Paul, D. R., & Robeson, L. M. (2008). Polymer nanotechnology: nanocomposites.
584 *Polymer*, 49(15), 3187-3204.

585 Pazmiño Betancourt, B.A., Douglas, J.F., & Starr F.W. (2013). Fragility and
586 cooperative motion in a glass-forming polymer-nanoparticle composite. *Soft Matter*
587 9, 241-254

588 Plazek, D. J., & Ngai, K. L. (1991). Correlation of polymer segmental chain dynamics
589 with temperature-dependent time-scale shifts. *Macromolecules* 24 (5), 1222−1224.

590 Qin, Q., & McKenna, B. (2006). Correlation between dynamic fragility and glass
591 transition temperature for different classes of glass forming liquids. *Journal of Non-*
592 *Crystalline Solids*, 352 (28-29), 2977−2985.

593 Ramadan, A. R., Esawi, A. M., & Gawad, A. A. (2010). Effect of ball milling on the
594 structure of Na^+-montmorillonite and organo-montmorillonite (Cloisite 30B).
595 *Applied Clay Science*, 47(3), 196-202.

596 Redondo-Foj, B., Carsí, M., Ortiz-Serna, P., Sanchis, M. J., Vallejos, S., García, F., &
597 García, J. M.(2014). Effect of the Dipole−Dipole Interactions in the Molecular
598 Dynamics of Poly(vinylpyrrolidone)-Based Copolymers. *Macromolecules*, 47,
599 5334−5346.

600 Rhim, J. W., Lee, S. B., & Hong, S. I. (2011a). Preparation and characterization of
601 agar/clay nanocomposite films: the effect of clay type. *Journal of Food Science*,
602 76(3), N40-N48.

603 Rhim, J. W. (2011b). Effect of clay contents on mechanical and water vapor barrier
604 properties of agar-based nanocomposite films. *Carbohydrate Polymers*, 86(2), 691-
605 699.

606 Rhim, J. W. (2012). Physical-Mechanical Properties of Agar/κ-Carrageenan Blend Film
607 and Derived Clay Nanocomposite Film. *Journal of Food Science*, 77(12), N66-N73.

608 Rhim, J. W., Park, H. M., & Ha, C. S. (2013a). Bio-nanocomposites for food packaging
609 applications. *Prog. Polym. Sci*., 38, 1629-1652.

610 Rhim, J. W. (2013b). Effect of PLA lamination on performance characteristics of
611 agar/κ-carrageenan/clay bio-nanocomposite film. *Food Research International*,
612 51(2), 714-722.

613 Rhim, J. W., & Wang, L. F. (2014). Preparation and characterization of carrageenan-
614 based nanocomposite films reinforced with clay mineral and silver nanoparticles.
615 *Applied Clay Science*, 97-98, 174-181.

Riande, E., & Díaz-Calleja, R. (2004). Electrical Properties of Polymers (New York: Dekker).

Rodriguez, S. A., Weese, E., Nakamatsu, J., & Torres, F. (2016). Development of Biopolymer Nanocomposites Based on Polysaccharides Obtained from Red Algae Chondracanthus chamissoi Reinforced with Chitin Whiskers and Montmorillonite. *Polymer-Plastics Technology and Engineering*, 55(15), 1557-1564.

Ryabov, Y.E., Nuriel, H., Marom, G., & Feldman, Y. (2003). Relaxation peak broadening and polymer chain dynamics in aramid-fiber-reinforced nylon-66 microcomposites. *Journal of Polymer Science* B *Polymer Physics*, 41(3), 217–223.

Sanchis, M. J., Domínguez-Espinosa, G., Díaz-Calleja, R., Guzmán, J., & Riande, E. (2008). Influence of structural chemical characteristics on polymer chain dynamics. *J. Chem. Phys.* 129, 054903.

Sanchis, M.J., Carsí, M. Gómez C.M., Culebras, M., Gonzales, K.N., & Torres, F.G. (2017). Monitoring molecular dynamics of bacterial cellulose composites reinforced with graphene oxide by carboxymethyl cellulose addition. *Carbohydrate Polymers* 157, 353–360

Sartori Pompeo da Silva, H., Ornaghi Junior, H. L., Santos Almeida Junior, J. H., Zattera, A. J., & Campos Amico, S. (2014). Mechanical Behavior and Correlation Between Dynamic Fragility and Dynamic Mechanical Properties of Curaua Fiber Composites. *Polymer Composite*, 35 (6), 1078-1086.

Sauti, G., & McLachlan, D. S. J. (2007). Impedance and modulus spectra of the percolation system silicon-polyester resin and their analysis using the two exponent phenomenological percolation equation. *Journal of Material Science*, 42 (16), 6477–6488.

Sengwa, R. J., Choudhary, S., & Sankhla, S. (2010). Dielectric properties of montmorillonite clay filled poly (vinyl alcohol)/poly (ethylene oxide) blend nanocomposites. *Composites Science and Technology*, 70(11), 1621-1627.

Shankar, S., Reddy, J.P., Rhim, J. & Kim, H. (2015). Preparation, characterization, and antimicrobial activity of chitin nanofibrils reinforced carrageenan nanocomposite films. *Carbohydrate Polymers*, 117, 468-475.

Shojaee-Aliabadi, S., Mohammadifar, M. A., Hosseini, H., Mohammadi, A., Ghasemlou, M., Hosseini, S. M., & Khaksar, R. (2014). Characterization of nanobiocomposite kappa-carrageenan film with Zataria multiflora essential oil and nanoclay. *International Journal of Biological Macromolecules*, 69, 282-289.

Tamman, G., & Hesse, W. (1926). Die Abhängigkeit der Viscosität von der Temperatur bie unterkühlten Flüssigkeiten. *Zeitschrift für Anorganische und Allgemeine Chemie*, 156, 245-247.

Tsangaris, G.M., Psarras, G.C., & Kouloumbi, N. (1998). Electric modulus and interfacial polarization in composite polymeric systems. *Journal of Materials Science*, 33, 2027-2037.

656 Tuvikene, R., Truus, K., Vaher, M., Kailas, T., Martin, G., & Kersen, P. (2006).
657 Extraction and quantification of hybrid carrageenans from the biomass of the red
658 algae Furcellaria lumbricalis and Coccotylus truncates. *Proc. Estonian Acad. Sci.*
659 *Chem.* 55, 40-53.

660 Van de Velde, F. (2008). Structure and function of hybrid carrageenans. *Food*
661 *Hydrocolloids*, 22(5), 727-734.

662 Vogel, H. (1921). The law of the relationship between viscosity of liquids and the
663 temperature. *Physikalische Zeitschrift*, 22, 645-646.

664 Wang, H-W., Chang, K-C., Yeh, J-M., & Liou, S-J. (2004). Synthesis and Dielectric
665 Properties of Polystyrene-Clay Nanocomposite Materials. *Journal of Applied*
666 *Polymer Science*, 91, 1368–1373.

667 Yi, X., Duan, H. L., Chen, Y., & Wang, J. (2007). Prediction of complex dielectric
668 constants of polymer-clay nanocomposites. *Physics Letters A*, 372(1), 68-71.